Key Points:
- Meteorology drives the seasonality of remote contributions to Arctic sulfate burden
- Sulfate radiative forcing can partly offset Arctic positive forcing from black carbon
- Sources in regions having short transport pathways and long lifetimes are more efficient in influencing Arctic radiation

Sulfate Aerosol in the Arctic: Source Attribution and Radiative Forcing

Yang Yang[1] (ID), **Hailong Wang[1]** (ID), **Steven J. Smith[2]** (ID), **Richard C. Easter[1]** (ID), and **Philip J. Rasch[1]** (ID)

[1]Atmospheric Science and Global Change Division, Pacific Northwest National Laboratory, Richland, WA, USA, [2]Joint Global Change Research Institute, Pacific Northwest National Laboratory, College Park, MD, USA

Abstract Source attribution of Arctic sulfate and its radiative forcing due to aerosol-radiation interactions (RFari) for 2010–2014 are quantified in this study using the Community Earth System Model equipped with an explicit sulfur source-tagging technique. The model roughly reproduces the seasonal pattern of sulfate but has biases in simulating the magnitude of near-surface concentrations and vertical distribution. Regions that have high emissions and/or are near/within the Arctic present relatively large contributions to Arctic sulfate burden, with the largest contribution from sources in East Asia (27%). Seasonal variations of the contribution to Arctic sulfate burden from remote sources are strongly influenced by meteorology. The mean RFari of anthropogenic sulfate offsets one third of the positive top of the atmosphere (TOA) RFari from black carbon. A 20% global reduction in anthropogenic SO_2 emissions leads to a net Arctic TOA forcing increase of +0.019 W m^{-2}. These results indicate that a joint reduction in BC and SO_2 emissions could prevent at least some of the Arctic warming from any future SO_2 emission reductions. Sulfate RFari efficiency calculations suggest that source regions with short transport pathways and meteorology favoring longer lifetimes are more efficient in influencing the Arctic sulfate RFari. Based on Arctic climate sensitivity factors, about −0.19 K of the Arctic surface temperature cooling is attributed to anthropogenic sulfate, with −0.05 K of that from sources in East Asia, relative to preindustrial conditions.

1. Introduction

Long-range transport of aerosols from Northern Hemisphere midlatitudes can increase Arctic aerosol concentrations (Breider et al., 2014; Fisher et al., 2011; Hegg et al., 2010; Shindell et al., 2008; Wang et al., 2013, 2014). Stable stratification in the Arctic prevents constituents emitted locally from reaching the free troposphere, leading to a more important role of local sources for near-surface aerosol concentrations. Due to extremely low temperatures at the surface and therefore frequent and persistent occurrences of surface temperature inversions, the Arctic lower troposphere is isolated from lower latitudes by a transport barrier called the "Arctic front," which shifts seasonally. For polluted air reaching the Arctic lower troposphere on timescales shorter than a few weeks, the source regions have to be located north of the Arctic front. In summer, due to the northerly location of the Arctic front, it is difficult for aerosols emitted into the relatively warm air masses in the south to move into the Arctic lower troposphere. They can reach the Arctic only by isentropic transport into the upper troposphere (Stohl, 2006).

Sulfate is the dominant aerosol component over the Arctic (Breider et al., 2014; Quinn et al., 2007). Shindell et al. (2008) examined the sensitivity of modeled Arctic aerosol concentrations to perturbations of year 2001 emissions in four major source regions and concluded that European emissions dominated Arctic sulfate concentrations near the surface and at 500 hPa, with contributions of 73% and 51%, respectively, while East Asia was the largest contributor (36%) at 250 hPa. Focusing on more source regions/sectors, Fisher et al. (2011) examined the source attribution of Arctic sulfate using a chemical transport model and year 2005 emissions. They found that West Asia (southwest Russia and Kazakhstan) emissions were a major contributor (30–45%) to wintertime Arctic sulfate with contributions mainly within 2 km above the surface, while Europe and East Asia had similar strong contributions to the springtime sulfate at all altitudes. Using the same model and emissions, Breider et al. (2014) found that anthropogenic sources accounted for 83% of the Arctic surface sulfate in winter and spring. Large uncertainties exist in the source attributions of Arctic sulfate that are associated with emissions and models. For instance, Shindell et al. (2008) reported a three times higher contribution from Europe to the Arctic surface sulfate concentration than East Asia, while Fisher et al. (2011) found a similar contribution between these two source regions with a different model and emission dataset.

The Arctic has warmed dramatically in recent decades, with temperature increasing at a rate of about twice as fast as the global mean value (Intergovernmental Panel on Climate Change 2013). As one of the important short-lived forcers of Arctic climate (Quinn et al., 2008), aerosols perturb the Arctic radiative balance by reflecting or absorbing radiation and modifying clouds. Absorbing aerosols (e.g., black carbon (BC)) in snow and ice can reduce surface albedo and increase snow/ice melt (Flanner et al., 2007; Jacobson, 2010; Qian et al., 2015), causing a positive forcing. Including aerosol climatic effects in climate models better reproduces Arctic warming (Law & Stohl, 2007; Quinn et al., 2008).

Arctic net aerosol forcing depends on the amount of absorbing versus scattering species and the net radiative effects of each. Modeling results reported by Quinn et al. (2008) show that anthropogenic sulfate exerted a negative radiative forcing due to aerosol-radiation interactions (RFari; i.e., aerosol direct effects) with a seasonal maximum of -0.54 W m^{-2} at the top of the atmosphere (TOA) and -0.50 W m^{-2} at the surface in summer, while BC exerted a maximum RFari of 1.2 W m^{-2} at the TOA and -0.39 W m^{-2} at the surface in spring. Modeling results of Flanner (2013) suggest a surface warming due to BC in the Arctic lower troposphere, in large part due to BC albedo effects on snow and ice, and a cooling due to BC in the Arctic upper troposphere. The meridional gradient of aerosols can also influence the Arctic by changing poleward heat transport. Without considering the effects of BC deposition on snow and ice, Shindell and Faluvegi (2009) found that increasing BC at low and midlatitudes leads to surface warming in the Arctic while increasing Arctic local BC resulted in surface cooling. Based on climate model simulations, Sand et al. (2013) pointed out that the Arctic surface warming induced by increased concentrations of BC in the midlatitudes was due to increased transport of heat into the Arctic. Arctic surface cooling induced by increased BC throughout the Arctic atmosphere was caused by a combination of weakened atmospheric northward heat transport, as well as changes in surface fluxes, and local feedbacks. Using an Earth system model, Acosta Navarro et al. (2016) reported that the reduction in Europe SO$_2$ emission over 1980–2005 has caused warming in the Arctic as a result of the enhanced poleward heat transport.

A better understanding of the sensitivity of Arctic radiation budgets to changes in anthropogenic SO$_2$ emissions from various source regions is, therefore, important for understanding Arctic climate. Anthropogenic emissions of SO$_2$ (i.e., the precursor of sulfate particles) have decreased drastically in developed countries in the past few decades (US Environmental Protection Agency, 2010; Vestreng et al., 2007). Air quality regulations have also become more effective in some developing countries, which has started to decrease SO$_2$ emissions in China in particular (van der A et al., 2017). Yang et al. (2014) reported a 1.8 K surface warming over the European Arctic in 2005, compared to 1975. Acosta Navarro et al. (2016) attributed 0.5 K warming to an additional 0.3 W m^{-2} reaching the Arctic surface from European reductions in SO$_2$ emissions since 1980. Breider et al. (2017) used a global chemical transport model to construct Arctic aerosols from 1980 to 2010 and found that aerosol-radiation interactions over the Arctic and midlatitudes roughly explained one quarter of the observed Arctic surface warming over this period. Fyfe et al. (2013) concluded that reproducing the observed multidecadal variation in Arctic surface temperature required accurate simulations of transport, deposition, and retention of anthropogenic sulfate.

SO$_2$ emissions are expected to continue decreasing in both developed and developing countries in the future (Rao et al. 2017). Wobus et al. (2016) used equilibrium temperature response factors to examine future temperature responses to aerosol emissions and pointed out that greenhouse gases mitigation could generate a short-term Arctic warming due to energy sector reductions in SO$_2$ emissions. Using an Earth system model, Gagné et al. (2015) reported that projected declines in aerosol emissions over the 21st century could result in a decrease in Arctic sea ice extent of 1×10^6 km^2. Stjern et al. (2016) also showed that aerosol emission reductions in Europe had strong impacts on RFari in the Arctic.

To our knowledge, few studies have focused on the attribution of Arctic sulfate forcing to individual source regions/sectors. Sand et al. (2016) used multimodel simulations of aerosol forcing to estimate the equilibrium response of Arctic surface air temperature to changes in year 2010 aerosol emissions. They found that, among the seven source regions (United States, Canada, Russia, the Nordic countries, rest of Europe, East and South Asia, and the rest of the world), sulfate originating from East and South Asia had the largest contribution to cooling in the Arctic, whereas the Arctic surface temperature is most sensitive (per unit emission) to emissions within or near the Arctic.

Here we use the Community Earth System Model (CESM) with an explicit sulfur tagging technique to quantify source-receptor relationships of Arctic sulfate. We examine a larger number of source regions than in previous work (e.g., Sand et al., 2016) including separation of East Asia and South Asia, both of which have strong contributions to global RFari of sulfate (Yang, Wang, Smith, Easter, et al., 2017). We also separate contributions from natural sources. Given that many models have shown difficulties in capturing sulfate over the Arctic (Koch et al., 2009; Shindell et al., 2008), quantifying sulfate source-receptor relationships over the Arctic can also help to attribute model bias.

Building on Yang, Wang, Smith, Easter, et al. (2017), we quantify source contributions from 16 different regions/sectors (covering the whole globe) to Arctic sulfate surface concentration, column burden, and RFari and identify the relative importance of emissions and meteorology in determining source contributions. The CESM model and numerical experiments are described in section 2. Section 3 compares the simulated Arctic sulfate mass concentrations with observations. Section 4 provides modeled source attributions of mass concentrations and column burden of Arctic sulfate to the tagged source regions/sectors. Section 5 examines source attribution of Arctic RFari of sulfate and RFari efficiency for individual source regions/sectors, the responses of sulfate RFari to a 20% uniform reduction in anthropogenic SO_2 emissions globally, and projected Arctic temperature responses to sulfate RFari. Section 6 summarizes the results of this study.

2. Methodology

Sulfate mass concentrations and RFari are simulated with the Community Atmosphere Model version 5 (CAM5), the atmospheric component of CESM. Mass and number concentrations of sulfate particles are predicted with the three lognormal modes (i.e., Aitken, accumulation, and coarse mode) of the modal aerosol module (Liu et al., 2012) in CAM5. Within each mode, sulfate is internally mixed with primary/secondary organic matter, BC, mineral dust, and/or sea salt. Optical properties of the aerosol mixture are parameterized according to Ghan and Zaveri (2007). In addition to the standard treatments of aerosol and aerosol-cloud interactions described by Neale et al. (2012), also included in our version of the model is a set of modifications that improves the simulation of aerosol wet scavenging and convective transport (Wang et al., 2013). In our model simulations, radiative transfer is calculated multiple times in order to diagnose the radiative impact of one or more aerosol components or certain species being tagged. The RFari is defined as the difference of all-sky net shortwave radiative fluxes between two diagnostic calculations, with and without the aerosols considered (Ghan, 2013). The model uses prognostic size distribution of aerosols based on a two-moment scheme. The size distribution of the remaining aerosol species with sulfate excluded from the mixture is calculated again in the diagnostic radiative calculation. Radiative forcing due to aerosol-cloud interactions is not analyzed in this study due to the large uncertainties in the treatment of the Arctic cloud and aerosol-cloud interactions in climate models (McFarquhar et al., 2011). The effects of light-absorbing particles (BC and dust) on snow and ice are included in the model (Flanner et al., 2007; Yang, Wang, Smith, Ma, et al., 2017).

To quantify source attributions of Arctic sulfate, we use the same sulfur source-tagging technique implemented in CAM5 by Yang, Wang, Smith, Easter, et al. (2017), in which sulfate and its precursor gases from independent source regions and sectors can be explicitly tracked. While Yang, Wang, Smith, Easter, et al. (2017) quantified global source-receptor relationships, source attribution over the Arctic was not considered in that work. Following Yang, Wang, Smith, Easter, et al. (2017), sulfur emissions from 14 anthropogenic geographical source regions are tagged: East Asia (EAS), Europe (EUR), North America (NAM), Russia/Belarus/Ukraine (RBU), South Asia (SAS), the Middle East (MDE), Pacific/Australia/New Zealand (PAN), North Africa (NAF), Central America (CAM), Central Asia (CAS), Southern Africa (SAF), South America (SAM), Southeast Asia (SEA), and the rest of the world (ROW, including oceans and polar continents). We also tagged two natural source sectors, oceanic dimethyl sulfide (DMS) and volcanic SO_2. The Arctic (180°W–180°E, 66.5°N–90°N) is the receptor region we focus on here. Note that Arctic local emissions are included in the ROW emission in this study. In a separate diagnostic simulation separating out Arctic local emissions from ROW (not shown), the Arctic local emissions contribute 97% of near-surface concentrations and 80% of the column burden for Arctic sulfate from ROW (including the Arctic) emission. The ROW region is, therefore, a reasonable proxy for Arctic emissions in the context of this study.

CAM5 simulations are conducted for years 2009–2014 with 1.9° (latitude) by 2.5° (longitude) horizontal grids and 30 vertical layers in the nudging mode (Ma et al., 2013; Zhang et al., 2014), in which wind fields are

nudged to the MERRA (Modern-Era Retrospective Analysis for Research and Applications) reanalysis (Rienecker et al., 2011) at a timescale of 6 h. The results of the last 5 years are analyzed hereafter. Both anthropogenic (version 20160726) and open fire (version 20161213) emissions used in our simulations are from the data sets released for the Coupled Model Intercomparison Project Phase 6 (Hoesly et al., 2018; van Marle et al., 2017). Climatologically averaged monthly volcanic SO_2 and DMS emissions were obtained from AeroCom (Diehl, 2009). It should be noted that the use of constant natural emissions may lead to inaccurate interannual variations of sulfate concentrations, RFari, and source contributions from natural emissions. In CAM5, SO_2 from energy and industry sectors is evenly distributed in the 100–300 m layer above the surface, while other anthropogenic sectors are emitted from the surface. Upon emission, 2.5% of sulfur is immediately transformed to sulfate particles in CAM5. Because open biomass burning SO_2 only accounts for less than 2% of the total (anthropogenic + open biomass burning) SO_2 globally, the total SO_2/sulfate are referred to as anthropogenic SO_2/sulfate hereafter. We performed a base simulation with full emissions and a sensitivity simulation with a uniform 20% reduction in anthropogenic SO_2 emissions globally. The latter is mainly used to quantify the impact of the emission reduction on Arctic source-receptor relationships.

Figure 1b shows the spatial distribution of anthropogenic SO_2 emissions averaged over 2010–2014, with the 14 tagged anthropogenic source regions marked in Figure 1a. The global total anthropogenic SO_2 emission rate is 57.7 Tg S yr^{-1}. The spatial variability is large. North America, Europe, and RBU, regions close to the Arctic, emit similar amounts of SO_2 over this period, with annual means of 3.1, 3.3, and 3.0 Tg S yr^{-1}, respectively. Among the major source regions in the midlatitude of the Northern Hemisphere, East Asia contributes 17.8 Tg S yr^{-1} of anthropogenic SO_2 emission, about one third of the global total value, followed by 6.4 Tg S yr^{-1} from South Asia, 3.4 Tg S yr^{-1} from the Middle East, and 1.1 Tg S yr^{-1} from Central Asia. Emissions from ROW contribute 11.2 Tg S yr^{-1} of SO_2, with 0.8 Tg S yr^{-1} contributed by the Arctic local emissions (mostly from the industry sector). Volcanic SO_2 and oceanic DMS from natural sources also contribute 12.6 and 18.2 Tg S yr^{-1} (Figures 1c and 1d). Although the remaining tagged source regions (CAM, SAM, NAF, SAF, SEA, and PAN) can have significant emissions, ranging from 0.6 to 2.7 Tg S yr^{-1}, these regions are too far away to exert a significant influence on Arctic aerosols (e.g., Wang et al., 2014). The seasonality of emissions from the tagged source regions/sectors has been described by Yang, Wang, Smith, Easter, et al. (2017).

3. Model Evaluation

To evaluate the model's ability in simulating Arctic sulfate, Figure 2 compares the simulated seasonal cycle of near-surface sulfate concentrations with observations at Barrow (note that the city of Barrow Alaska is now called Utqiaġvik; 71°N, 156°W), Zeppelin (78°N, 11°E), Alert (82°N, 62°W), and Trapper Creek (62°N, 150°W) sites in the Arctic. Site locations are shown in Figure 1a. Note that model results are averaged between 2010 and 2014, while observations represent the mean of certain years within 1997–2009, which may lead to discrepancies between model and observations.

The observed sulfate concentrations over the Arctic generally reach their peak in boreal winter and spring and trough in summer and autumn. The model roughly reproduces the seasonal pattern at the Barrow site but simulates a shifted seasonal peak to late spring and early summer at the Zeppelin and Trapper Creek sites and strongly underestimates the seasonal peak in spring at the Alert site. Sulfate at the Alert site is underestimated by a large amount in winter and spring compared to the observations, which was also reported by other modeling studies (Breider et al., 2014; Eckhardt et al., 2015; Fisher et al., 2011). Arctic aerosol concentrations have large spread among models. Previous multimodel intercomparison studies (Koch et al., 2009; Shindell et al., 2008) reported large differences between simulated and observed Arctic aerosol concentrations (e.g., sulfate and BC), including incorrect seasonality and orders-of-magnitude biases. With sulfate source tagging technique, we can improve analysis of these biases as discussed in sections 4 and 6 below.

Figure S1 in the supporting information compares the vertical profiles of sulfate during the ARCTAS campaign in April and July 2008 near the North American Arctic (Jacob et al., 2010). The modeled 2010–2014 average profiles reproduce the larger concentrations in July than in April. The model and observations agree around 5 km. However, the model overestimates near-surface sulfate concentrations in April but underestimates in July, perhaps due to uncertainties in local SO_2 emissions, natural DMS emissions, or model
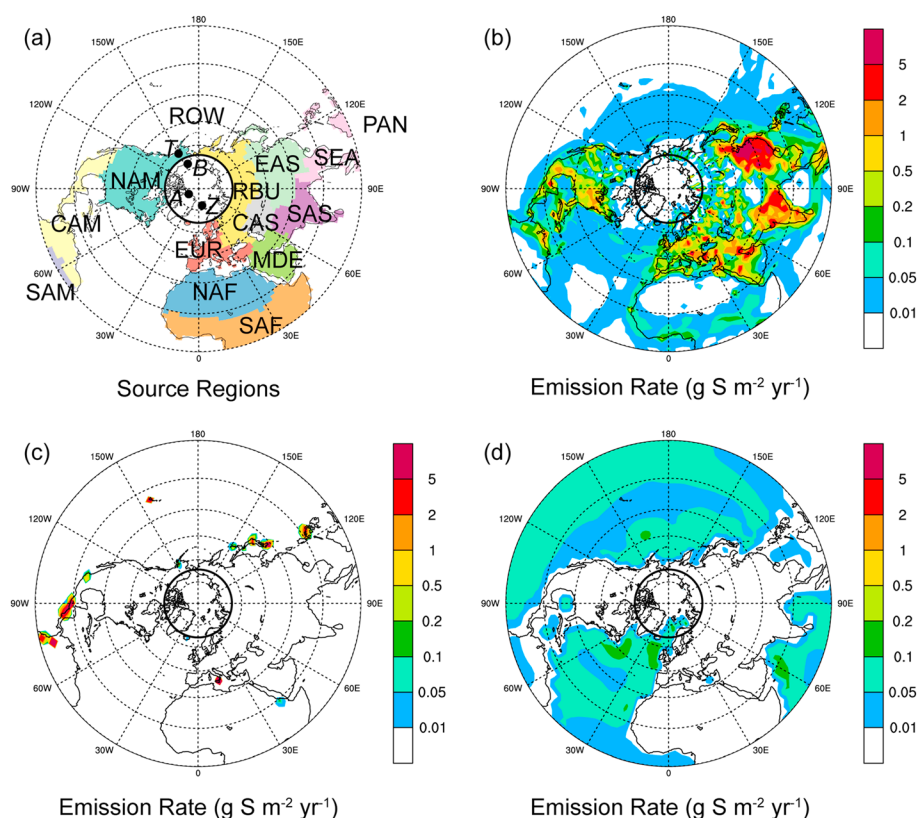
Figure 1. (a) Tagged source regions (EAS: East Asia, EUR: Europe, NAM: North America, RBU: Russia/Belarus/Ukraine, SAS: South Asia, MDE: the Middle East, PAN: Pacific/Australia/New Zealand, NAF: North Africa, CAM: Central America, CAS: Central Asia, SAF: Southern Africa, SAM: South America, SEA: Southeast Asia, and ROW: rest of the world). Spatial distribution of annual mean emissions of (b) anthropogenic SO_2, (c) volcanic SO_2, and (c) oceanic DMS (g S m^{-2} yr^{-1}) averaged over 2010–2014. The thick black line marks the Arctic cycle at 66.5°N. Dots in (a) are observational sites over Barrow ("B," 71°N, 156°W), Zeppelin ("Z," 78°N, 11°E), Alert ("A," 82°N, 62°W), and Trapper Creek ("T," 62°N, 150°W).

parameterizations. At 8 km, the model overestimates sulfate concentrations in both April and July indicating that sulfate transported from distant sources to the Arctic is probably overestimated in this simulation. Based on the source-receptor relationships discussed below, both the Arctic and North American Arctic (not shown) sulfate concentrations around 8 km are mainly attributed to emissions from East Asia. This indicates a possible overestimation of SO_2/sulfate transported from East Asia at high altitudes over the Arctic. Given that we did not simulate the year 2008, we note that meteorological conditions specific to that year might also contribute to differences.

Figure 3 compares June-July-August (JJA) mean column burden of SO_2 derived from the Ozone Monitoring Instrument (OMI; Li et al., 2013) and the model simulation. Uncertainties in satellite data include cloud contamination, reduced satellite sensitivity to SO_2 in the presence of aerosols, priori assumptions in the retrieval algorithm for the vertical distribution of SO_2, and spatial sampling bias in the satellite data. One specific issue with the model simulation is less efficient oxidation of SO_2 in the model, which may have resulted in an overestimate of SO_2 concentrations in China in particular (Yang, Wang, Smith, Easter, et al., 2017). However, the model captures well the spatial distribution of SO_2 burden in the Arctic with large values near RBU Arctic. We cannot make reliable quantitative comparisons over the Arctic, however, because almost none of the Arctic OMI data pixels exceed the ~0.5 Dobson unit retrieval noise level (Li et al., 2013).

4. Source Attribution of Arctic Sulfate

Figure 4 shows the annual mean sulfate column burden contribution from each tagged source region/sector. Relative contributions are presented in Figure 5. Source regions with strong emissions or near/within the
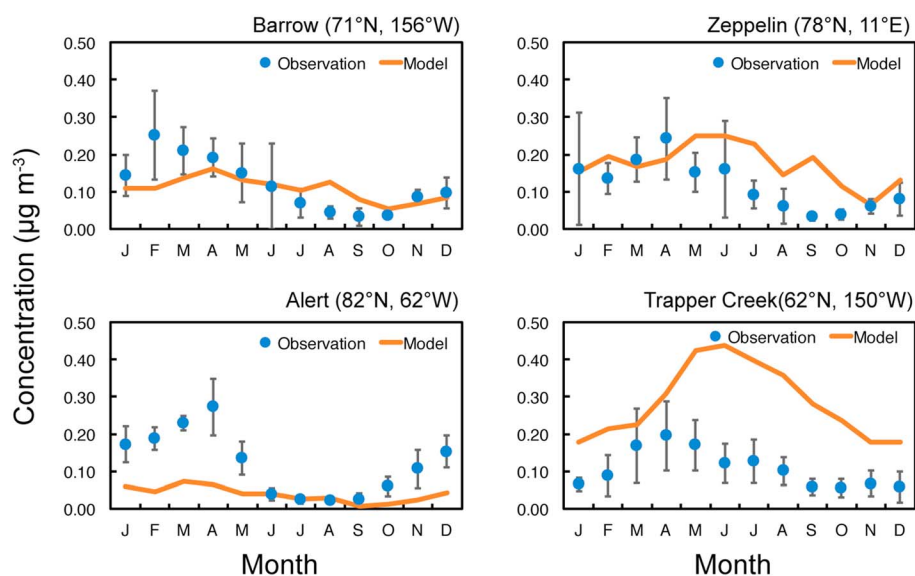
Figure 2. Seasonal variation of observed near-surface sulfate concentrations ($\mu g \ m^{-3}$) at Arctic sites of Barrow for 1997–2008, Zeppelin for 1999–2008, Alert for 1998–2008, and Trapper Creek for 2001–2009, along with model values at each site for 2010–2014. Observed concentrations are from the NOAA Pacific Marine Environmental Laboratory (http://saga.pmel.noaa.gov/data/) for Barrow site, EMEP (http://ebas.nilu.no) for Zeppelin site, Environment Canada (Gong et al., 2010) for Alert site, and IMPROVE (http://vista.cira.colostate.edu/improve/) for Trapper Creek site.

Arctic have large contributions to the Arctic sulfate burden. The simulated annual mean sulfate column burden over the Arctic is 2.19 mg m^{-2}, with the largest contribution of 0.59 mg m^{-2} (27%) from East Asia emissions. Sources from South Asia, ROW (largely local Arctic sources; section 2 above), and RBU each contribute 11–13% of the Arctic sulfate column burden. North America, Europe, the Middle East, and Central Asia each contribute 3–7%. Natural sources from volcanic activities (7%) and oceanic DMS (6%) together account for 13% of the sulfate over the Arctic. The remaining source regions do not have a substantial influence (total contribution less than 3%) on Arctic sulfate burdens due to their weak emissions and/or long transport pathways. Although anthropogenic sources (including fire emissions) dominate the Arctic sulfate burden, natural sources are not negligible.

Figure S2 shows the source contributions to the annual mean near-surface sulfate concentrations, and the relative contributions are presented in Figure S3. Compared to the sulfate column burden, contributions to the Arctic near-surface sulfate concentration decrease dramatically from the remote source regions of South Asia and East Asia and increase from 13% to 52% from the source region RBU. This indicates that
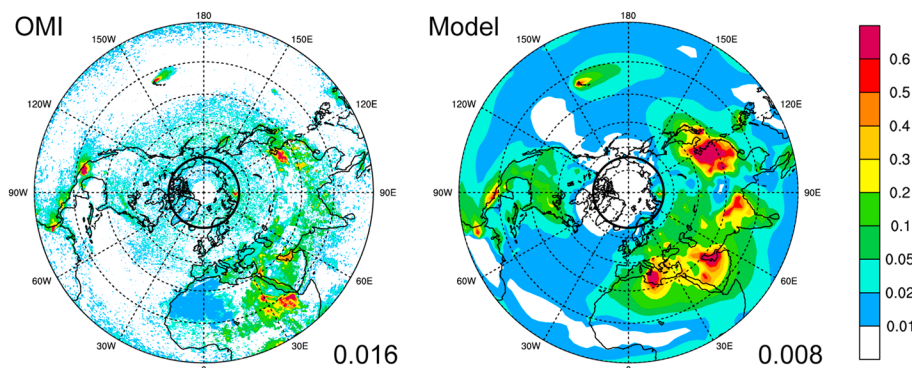

Figure 3. Spatial distribution of June-July-August (JJA) mean column burden of SO$_2$ (units: Dobson unit) derived from Ozone Monitoring Instrument (OMI) measurements (left panel) and model (right panel) over years of 2010–2014.
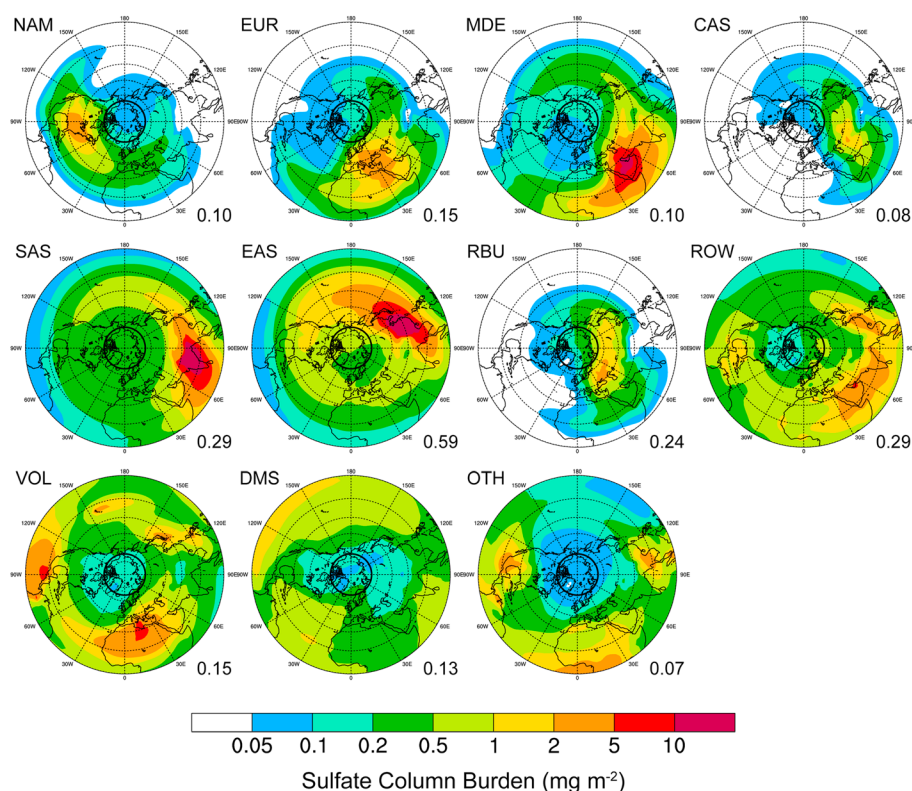
Figure 4. Spatial distribution of contributions to annual mean column burden of sulfate (mg m^{-2}) from the tagged source regions/sectors. Mean contributions to the Arctic sulfate from individual source regions/sectors are shown at the bottom right of each panel. Sources with relative contributions less than 1% are combined and shown as OTH (other).

the length of the transport pathway plays an important role in the source contributions to Arctic sulfate at different heights.

Table 1 summarizes seasonal relative contributions from the tagged source regions/sectors to the Arctic sulfate. The strong seasonal variability in the contributions from particular source regions is determined by variability in both seasonal emission rates and meteorology (Eckhardt et al., 2015; Garrett et al., 2011; Shaw, 1995; Shindell et al., 2008; Stohl, 2006; Wang et al., 2013). The relative contribution to the Arctic sulfate column burden from South Asia emissions shows a seasonal peak in December-January-February (DJF) and September-October-November (SON), with a value of 20%, compared to 8% in March-April-May (MAM) and JJA, even though the source emissions from South Asia present very small seasonal variability (1%). Table S1 presents the sulfate column burden efficiency, which is defined as the seasonal mean contribution to the Arctic sulfate column burden divided by the corresponding SO$_2$ emissions. The column burden efficiency for South Asia in DJF/SON is about twice that in MAM/JJA, suggesting that each unit SO$_2$ emission from South Asia in DJF/SON leads to a doubled contribution to the Arctic sulfate column burden as compared to a unit emission in MAM/JJA. This seasonality is likely due to strong removal during transport to the Arctic in MAM/JJA, rather than local wet removal or regional chemistry in the source region, because the sulfate burden averaged over South Asia in MAM/JJA (17–24 mg m^{-2}) is similar to or even higher than that in DJF/SON (15–19 mg m^{-2}).

Another example is RBU emissions, whose contribution to the Arctic sulfate burden is the largest in JJA (17%), twice as much as in DJF and SON, while the emission rate has a seasonal trough in JJA. The column burden efficiency for RBU shows a maximum in JJA and a minimum in DJF and SON, confirming the dominant role of meteorology in influencing the seasonality of column burden contributions from RBU. Considering that the sulfate burden averaged over RBU in JJA (4.7 mg m^{-2}) is also larger than that in DJF and SON (2.1–3.0 mg m^{-2}), the higher JJA contribution is likely due to higher temperatures that increase gas-phase reaction rates and oxidant concentrations in JJA, leading to the higher local sulfate concentrations (Dawson et al., 2007). In contrast, the Arctic near-surface concentration efficiency (Table S1) from
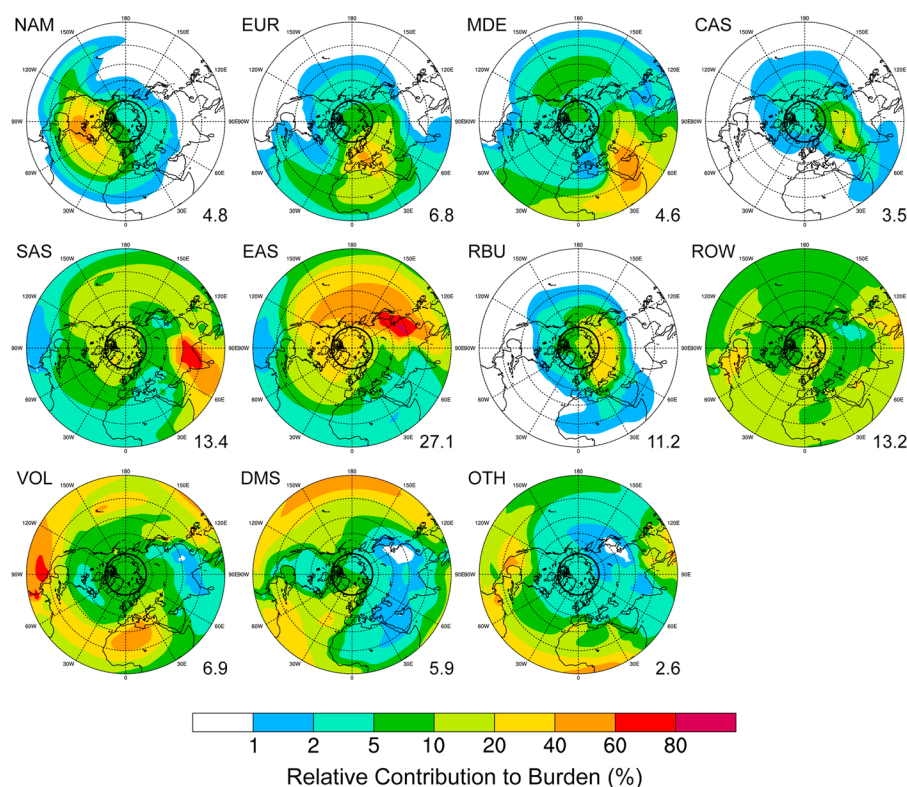
Figure 5. Spatial distribution of relative contributions (%) to annual mean sulfate column burden from each of the tagged source regions/sectors. Relative contributions to the Arctic mean burden from individual source regions/sectors are shown at the bottom right of each panel. Sources with relative contributions less than 1% are combined and shown as OTH (other).

RBU is similar in JJA and MAM, which is due to offsetting effects of different seasonal near-surface transport conditions, such as the location of the polar front. Sources in North America account for 9% of the Arctic sulfate column burden in JJA and 3–4% in other seasons, which largely reflects the higher JJA column burden efficiency for North America.

The contribution from East Asia emissions to the Arctic sulfate burden is four times larger than that from Europe in MAM in this study. This is different from Fisher et al. (2011) who found that Europe and East Asia have similar contributions in spring based on a chemical transport model simulation with year 2005 emissions. The difference is due to the different domain of source regions defined and time periods. Their Europe region (including parts of Russia) is larger than that in this study, leading to higher SO_2 emissions (6.9 Tg S yr^{-1} for 2008 from EMEP inventory) than in this study (4.2 Tg S yr^{-1} for 2008 and 3.3 Tg S yr^{-1} averaged during 2010–2014 for our smaller Europe region). Also, their East Asia domain includes our source regions East Asia, South Asia, and Southeast Asia, leading to a higher SO_2 emission (23 Tg S yr^{-1} for 2008 from the INTEX-B inventory) than the smaller East Asia source region in this study (17.8 Tg S yr^{-1} for 2008 and 17.6 Tg S yr^{-1} averaged during 2010–2014 from the Coupled Model Intercomparison Project Phase 6 emission inventory). Another reason could be that all SO_2 was emitted from the surface (bottom layer) in the model used by Fisher et al. (2011), while in our CAM5 simulation, SO_2 from energy and industry sectors is evenly distributed in the 100–300 m layer above the surface, favoring further lifting to the free troposphere and long-range transport. Therefore, it is important to know the source region domain and the treatment of emissions when comparing source attributions between different studies.

We now consider surface concentrations. Relative contributions to Arctic near-surface sulfate concentrations are also shown in Table 1. Emissions from ROW, which includes the Arctic local emissions, have the largest contribution among the tagged source regions/sectors, accounting for about 50% of the near-surface concentration of Arctic sulfate. Sources from RBU contribute 31% in DJF, likely associated with the strong northward transport in winter (Sharma et al., 2006). Oceanic DMS contributes 18% in JJA, largely due to the boreal

Table 1

Relative Contributions (%) From the Tagged Source Regions/Sectors to Mean Column Burden and Near-Surface Concentration of Sulfate Over the Arctic in December-January-February (DJF), March-April-May (MAM), June-July-August (JJA), and September-October-November (SON) and Annual Mean (ANN)

Contributions to sulfate column burden							
	NAM	CAM	SAM	EUR	NAF	SAF	MDE	SEA
DJF	2.7	0.8	0.2	6.8	0.6	0.3	4.5	1.0
MAM	3.3	0.6	0.2	7.2	0.8	0.3	7.4	0.7
JJA	9.2	0.7	0.2	7.5	0.4	0.3	2.3	0.8
SON	4.4	0.9	0.1	5.5	0.4	0.2	3.2	0.8
ANN	4.8	0.7	0.2	6.8	0.6	0.3	4.6	0.8
	CAS	SAS	EAS	RBU	PAN	ROW	VOL	DMS
DJF	3.2	18.0	25.2	8.6	0.0	14.1	7.9	6.0
MAM	4.0	8.3	28.5	11.2	0.0	12.4	8.7	6.4
JJA	3.3	8.0	23.5	16.6	0.0	15.5	5.6	6.0
SON	3.2	21.9	30.4	8.2	0.0	11.4	4.6	4.8
ANN	3.5	13.4	27.1	11.2	0.0	13.2	6.9	5.9

Contributions to near-surface sulfate concentration							
	NAM	CAM	SAM	EUR	NAF	SAF	MDE	SEA
DJF	2.0	0.0	0.0	5.4	0.1	0.0	0.9	0.0
MAM	2.2	0.1	0.0	3.7	0.1	0.0	1.0	0.0
JJA	5.1	0.1	0.0	3.9	0.1	0.0	0.6	0.0
SON	2.4	0.1	0.0	6.5	0.1	0.0	0.6	0.0
ANN	2.9	0.1	0.0	4.7	0.1	0.0	0.8	0.0
	CAS	SAS	EAS	RBU	PAN	ROW	VOL	DMS
DJF	7.1	0.4	3.5	30.7	0.0	46.2	1.1	2.5
MAM	2.9	0.4	5.7	17.5	0.0	54.4	1.9	10.1
JJA	1.3	0.2	3.4	14.4	0.0	50.9	1.6	18.3
SON	2.9	0.2	3.1	19.3	0.0	56.8	1.5	6.5
ANN	3.6	0.3	4.1	20.4	0.0	51.8	1.6	9.7

Note. CAM = Central America; CAS = Central Asia; DMS = oceanic dimethyl sulfide; EAS = East Asia; EUR = Europe; MDE = the Middle East; NAF = North Africa; NAM = North America; PAN = Pacific/Australia/New Zealand; RBU = Russia/Belarus/Ukraine; SAF = Southern Africa; SAM = South America; SAS = South Asia; SEA = Southeast Asia; ROW = rest of the world; VOL = volcanic SO_2

summer maximum DMS emissions in Northern Hemisphere high latitudes. Anthropogenic sources combined account for more than 80% of the annual Arctic near-surface sulfate concentration and 88% in MAM, similar to the value of 83% in spring reported by Breider et al. (2014).

To examine the possible reasons for biases in simulated Arctic near-surface sulfate concentrations compared to the observations, Table S2 presents the relative contributions to the sulfate concentrations over the four sites compared in this study (Figure 2). In JJA, DMS contributes more than half of the surface sulfate at the Zeppelin site. The simulated high value in JJA could, therefore, be due to an overestimation of DMS emissions.

At the Trapper Creek, Alaska site, North America is the largest contributor to the surface sulfate in JJA and the dominant anthropogenic source. The large overestimate of surface sulfate at this site is, therefore, likely due to an overestimation of the North America contribution. The major SO_2 sources in North America are directly measured and have a relatively low uncertainty (Smith et al., 2011). The differences at this site, therefore, are likely due to either regional to local sources not well resolved in the global inventory or biases in parameterizations, transport, and/or sulfate production rates impacting emissions from North America in particular. The topography near this site is complex with nearby large mountain peaks. The relatively low model resolution used in this study might not be able to accurately represent this particular site. While the summer Trapper Creek overestimate is consistent with the differences with ARCTAS (Figure S2), Trapper Creek does not show the same April surface underestimate seen in the ARCTAS comparison. Note also that the model agrees much better with surface observations at the more northern Barrow site (on the Arctic Ocean), where there is no dominant source region (Table S2) and the local topography is less complex.
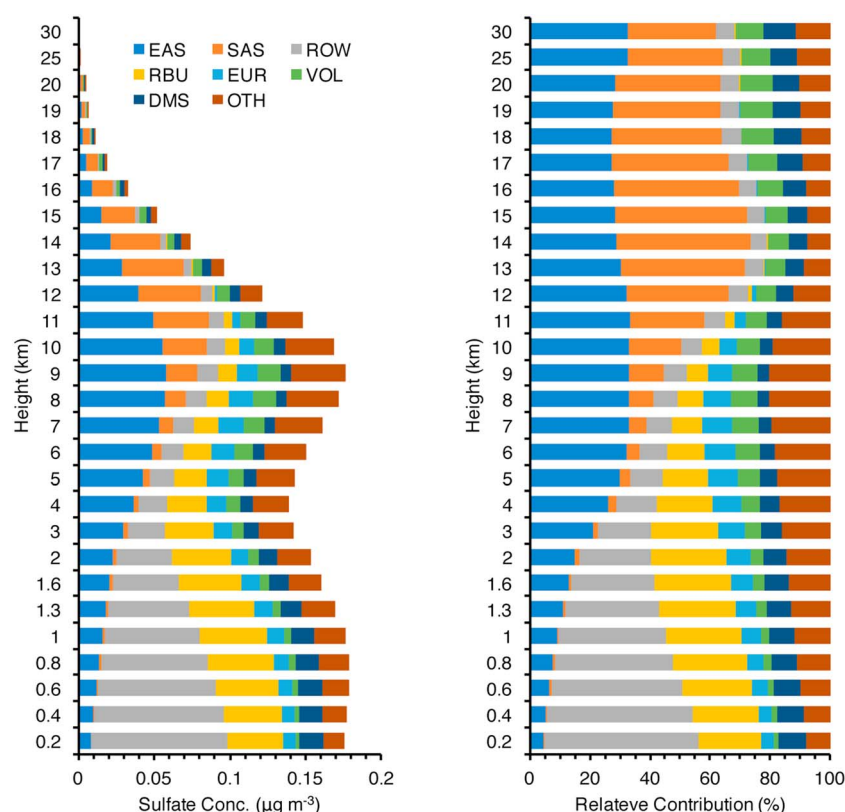
Figure 6. Annual mean vertical profile of sulfate concentrations ($\mu g\ m^{-3}$) over the Arctic contributed by the tagged source regions/sectors (left) and their relative contributions (right). Sources with annual burden contributions less than 5% are combined and shown as OTH (other).

At the Alert site, the model catches the minimum in JJA, but strongly underestimates the concentrations in other seasons. EAS, RBU, and ROW together account for 65% of surface concentrations in MAM at this site. Either emissions or transport from these regions likely account for this difference. We return to these comparisons in the discussion.

Note that model results are averaged between 2010 and 2014, while observations represent the mean of certain years within 1997–2009. However, if concentrations are scaled by the ratio of emission over the years of observation to 2010–2014 emission from each source region, the results are similar, except for the Trapper Creek site where the discrepancy increases (Figure S4).

Figure 6 shows the vertical distribution of Arctic annual mean sulfate concentrations from the tagged source regions/sectors, and Table S3 summarizes these values. Different source regions have very distinct vertical distributions of Arctic sulfate. East Asia and South Asia have their maximum contributions at 9–12 km, accounting for about one third of the Arctic sulfate concentrations in that height range, similar to the finding of Shindell et al. (2008), whereas emissions from ROW (dominated by the Arctic in this case) account for half of the Arctic sulfate at the surface and more than a quarter below 2 km. Another quarter below 2 km is contributed by RBU emissions. European emissions have relatively small contributions at all levels with a peak around 7 km, contributing 10% of the sulfate at this altitude. Natural volcanic emissions have a large contribution (20%) at about 8 km due to high-altitude emission injection, while oceanic DMS emitted from the ocean surface has a moderate contribution (8–9%) below 2 km. These local and remote sources lead to the two peaks of Arctic sulfate concentrations located below 1 km and around 9 km, respectively. The vertical profile would be expected to change over time as the relative emission levels in source regions vary. Figure S5 provides the seasonal mean source contributions to the vertical distributions. In DJF, due to the more southerly location of the Arctic front, it is easier for nearby aerosols (e.g., RBU) to move into the Arctic lower troposphere compared to other seasons. This leads to a maximum contribution from RBU located at lower altitudes in DJF, compared to other seasons. Due to stronger production of sulfate in East
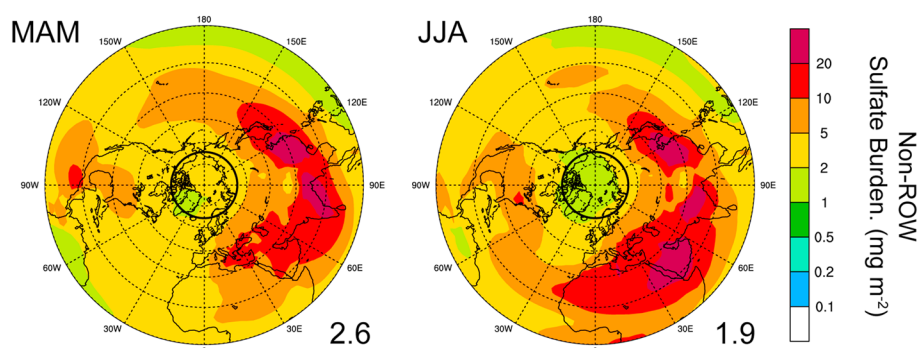
Figure 7. Spatial distribution of sulfate burden (mg m^{-2}) contributed by the non-ROW emissions in MAM and JJA.

Asia in MAM relative to DJF and easier transport to the Arctic in MAM relative to JJA, East Asia has a large contribution around 7 km in MAM. Lower precipitation and easier transport leads to a high South Asia contribution in DJF and SON around 13 km. These suggest an influence of meteorology on the seasonality of aerosol transport from nonlocal sources to the Arctic.

Figure 7 presents the spatial distribution of Arctic sulfate burden originating from non-ROW sources in MAM and JJA separately. The sulfate burden in JJA is higher compared to MAM in many regions outside the Arctic (e.g., the Middle East, North America, North Atlantic Ocean, and North Africa). However, non-ROW source contributions to the Arctic sulfate burden are lower in JJA (1.9 mg m^{-2}) than in MAM (2.6 mg m^{-2}) due to the northerly location of the Arctic front in summer, blocking aerosols from outside the Arctic. This illustrates that the seasonal variation of remote source contributions to the Arctic sulfate burden is primarily driven by the seasonality of meteorology, such as the location of the Arctic front.

5. Arctic Sulfate RFari and Efficiency

To quantitatively highlight the role of sulfate aerosol in affecting the Arctic radiative balance, Figure 8 compares the annual mean RFari of BC, radiative forcing due to BC in snow (calculated in the same simulation as that for sulfate) and sulfate RFari at the surface and the TOA. Scattering and absorption of solar radiation by BC particles produce a negative RFari of -0.08 W m^{-2} at the surface. BC deposited on snow can also absorb solar radiation and leads to an Arctic-average positive surface forcing of 0.16 W m^{-2}. When adding these two effects, BC exerts a net positive radiative forcing of 0.08 W m^{-2} at the Arctic surface. Sulfate produces a negative RFari of -0.08 W m^{-2} at the Arctic surface, with -0.07 W m^{-2} contributed by anthropogenic emissions, offsetting nearly all of the positive forcing at the surface from BC. At the Arctic TOA, atmospheric BC has a positive RFari of 0.27 W m^{-2}. Sulfate contributes a negative TOA RFari of -0.09 W m^{-2}, with -0.08 W m^{-2} contributed by anthropogenic emissions.

The TOA RFari of atmospheric BC simulated in this study is on the low end of the forcing range of 0.30 to 0.66 W m^{-2} reported in previous studies (AMAP, 2015; Breider et al., 2017; Quinn et al., 2008), and the sulfate TOA RFari is also weaker than those (-0.10 to -0.60 W m^{-2}) reported in previous studies (AMAP, 2015; Breider et al., 2017; Myhre et al., 2013; Quinn et al., 2008). The weaker RFari of sulfate simulated in this study is due in part to the different latitude range of the Arctic used here. In this study, the Arctic is defined as 66.5°N–90°N, while most previous studies used 60°N–90°N. Within the 60°N–66.5°N band, aerosol loading and insolation are usually stronger than the average over 66.5°N–90°N. The TOA RFari of anthropogenic sulfate over 60°N–90°N in this study is -0.13 W m^{-2}, while the TOA RFari of atmospheric BC is 0.29 W m^{-2}. The 2010–2014 BC and sulfate TOA forcing are 7% and 63% larger for the 60°N–90°N region as compared to the 66.5°N–90°N region. When considering a larger Arctic region, the area-average forcing of sulfate increases substantially in these results, while that for BC does not change as much. This means that negative sulfate forcing offsets a larger portion of positive BC forcing at TOA in the lower latitude portions of the Arctic.

Most of the previous studies used emissions before 2010, while in this study, emissions are for 2010–2014 when substantial reductions occurred in Europe, North America, and Russia. However, if forcing is scaled
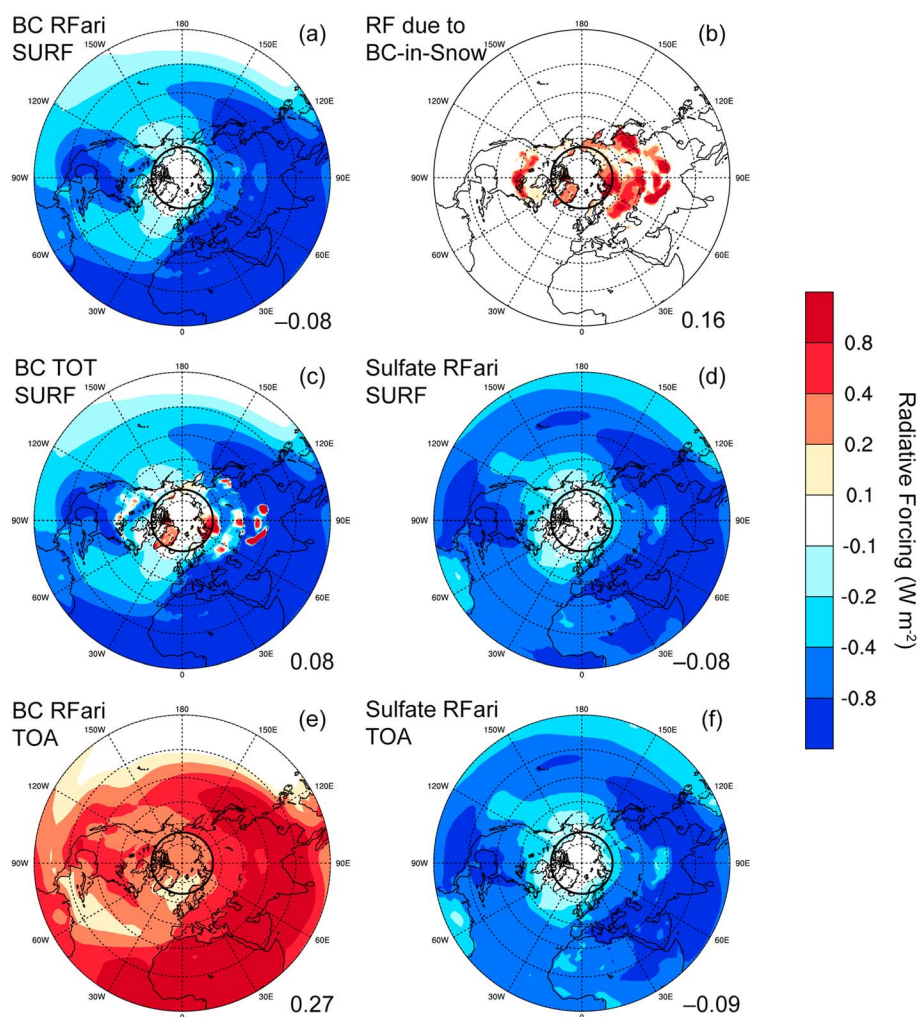
Figure 8. Spatial distribution of annual mean (a) black carbon (BC) radiative forcing due to aerosol-radiation interactions (RFari), (b) radiative forcing (RF) due to BC in snow, (c) BC total RF, and (d) sulfate RFari (W m^{-2}) at the surface, as well as (e) BC and (f) sulfate RFari at the TOA. Values averaged over the Arctic are shown at the bottom right of each panel.

by the ratio of 2003–2007 (representing 2005 level) to 2010–2014 emissions from each source region, the anthropogenic sulfate RFari over the Arctic (66.5°N–90°N) TOA is −0.09 W m^{-2}, only slightly smaller than the value we obtain for 2010–2014.

Quinn et al. (2008) simulated an annual mean Arctic sulfate RFari of −0.2 W m^{-2}, which is 53% larger than our value over the 60°N–90°N region but still much lower than −0.6 W m^{-2} reported by Breider et al. (2017). Sulfate burden in spring (MAM) was 40% higher than that in summer (JJA) in Quinn et al. (2008), whereas MAM burden was about 100% higher than JJA in Breider et al. (2017). In our study, Arctic sulfate burden (66.5°N–90°N) is 2.8 mg m^{-2} in MAM, which is also only 40% higher than 2.0 mg m^{-2} in JJA. Our annual mean sulfate burden of 2.2 mg m^{-2} is lower than 3.0 mg m^{-2} in Breider et al. (2017), partly explaining the lower sulfate RFari simulated in our study. Another important factor affecting all-sky sulfate RFari is the presence of clouds. If the forcing calculation uses clear-sky radiative fluxes in our model results, anthropogenic sulfate RFari changes from −0.08 to −0.20 W m^{-2} in 66.5°N–90°N and from −0.13 to −0.31 W m^{-2} in 60°N–90°N. It indicates that model-simulated all-sky aerosol forcing strongly depends on cloud properties, which can also contribute to differences between modeling studies. Note that sulfate indirect radiative forcing due to aerosol-cloud interactions, which is not analyzed here, may lead to an additional negative radiative forcing. These findings indicate that sulfate aerosol may be as important as BC in influencing the Arctic climate.
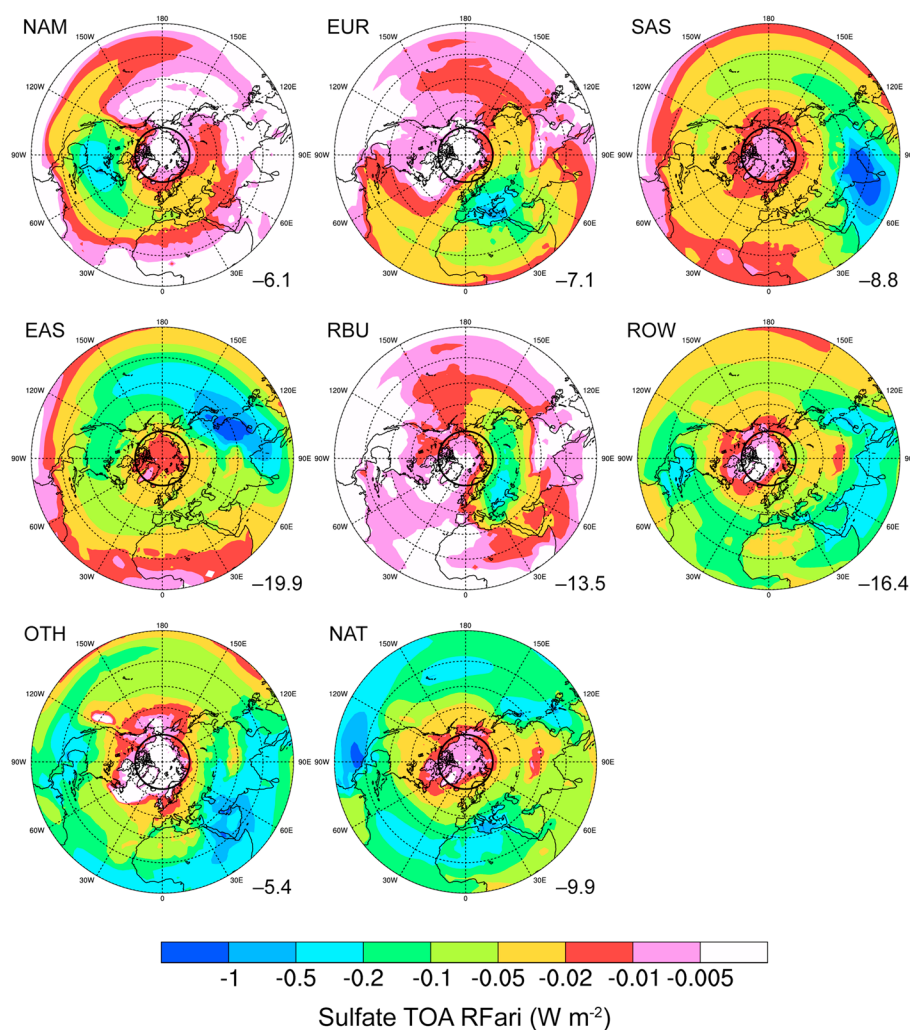
Figure 9. Spatial distribution of contributions to annual mean RFari of sulfate (W m^{-2}) at the TOA from the tagged source regions/sectors. Contributions to sulfate RFari (mW m^{-2}) averaged over the Arctic from individual source regions/sectors are shown at the bottom right of each panel. Sources with magnitude of annual Arctic anthropogenic sulfate RFari less than -5 mW m^{-2} are combined and shown as OTH. Natural sources of DMS and VOL are combined and shown as NAT.

Figure 9 shows the source contributions to the annual mean TOA sulfate RFari. Contributions to the Arctic sulfate RFari are higher for sources with higher burden contributions (Figure 4). Anthropogenic sources from East Asia, ROW (largely Arctic), and RBU contribute -0.020, -0.016, and -0.014 W m^{-2}, respectively, followed by North America, Europe, and South Asia, contributing between -0.006 and -0.009 W m^{-2}. Natural sources including oceanic DMS emissions and volcanic emissions account for -0.010 W m^{-2}. Interestingly, although South Asia is the second largest contributor to the annual Arctic sulfate burden, its contribution to the annual Arctic sulfate RFari is relatively small. This is because the seasonal contributions of South Asia emissions to Arctic sulfate are out of phase with insolation. In JJA when insolation is the strongest, sulfate burden contributed from the South Asia source reaches its minimum (Table 1), leading to the weak annual mean RFari.

Figure 10a shows seasonal source contributions to the Arctic sulfate TOA RFari. Almost all source regions/sectors show largest contributions in JJA when insolation is strong, while smallest in DJF when almost no solar radiation reaches the Arctic. In JJA, emissions from the distant East Asia, neighboring sources from RBU, and local Arctic sources (ROW) have similar contributions of -0.035 to -0.045 W m^{-2} to Arctic sulfate RFari, indicating that both location and emission source strength are important. Sources from North America, Europe, and South Asia and natural sources each add about -0.015 to -0.020 W m^{-2} in JJA. In MAM, all major sources (excluding South Asia) show the second largest contributions to the Arctic sulfate
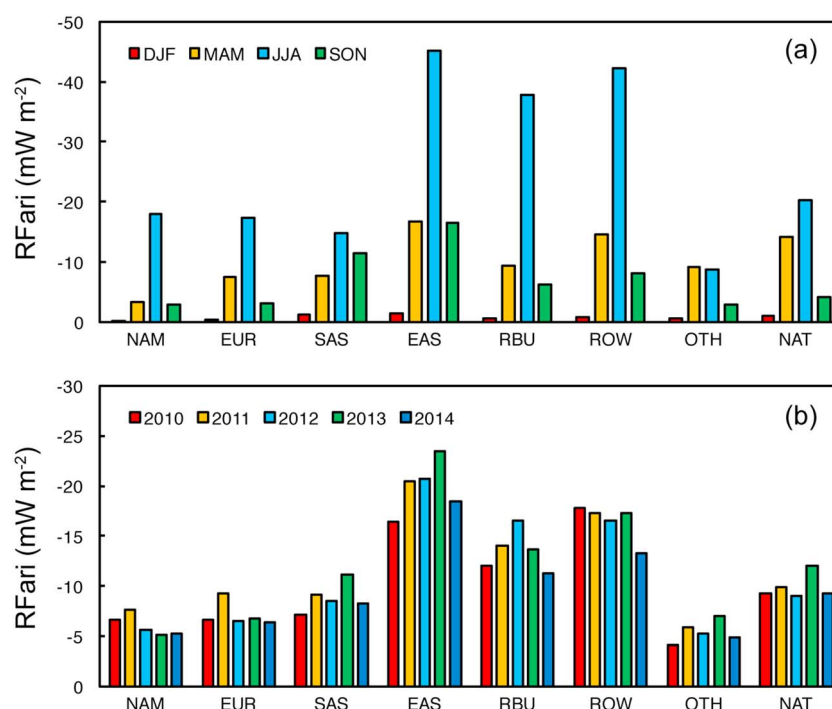
Figure 10. (a) Seasonal and (b) interannual variations of contributions of Arctic sulfate RFari (mW m^{-2}) from individual source regions/sectors at the TOA. Sources with magnitude of annual Arctic anthropogenic sulfate RFari less than -5 mW m^{-2} are combined and shown as OTH. Natural sources of DMS and VOL are combined and shown as NAT.

RFari. The Arctic total sulfate RFari at the TOA are -0.20 and -0.08 W m^{-2} in JJA and MAM, respectively. BC exerts maximum RFari at the TOA of $+0.50$ W m^{-2} in JJA and MAM. The similar BC RFari in MAM and JJA is due to a compensation between changes in BC burden and solar radiation. Transport of BC from remote source regions in JJA is less than in MAM because of the northerly location of the Arctic front and efficient wet scavenging during transport (e.g., Garrett et al., 2011; Mahmood et al., 2016; Stohl, 2006), while insolation over the Arctic is stronger in JJA. The different seasonality between BC and sulfate forcing is also due to the influence of the albedo of underlying surface on light absorption by atmospheric BC. The lower surface albedo over the Arctic in JJA than MAM leads to a smaller BC RFari in JJA. These again indicate that sulfate can be important in influencing the Arctic climate, especially in summer.

Figure 10b presents the interannual variation of source contributions to the annual Arctic sulfate RFari at the TOA during 2010–2014, summarized in Table S4 along with regional sulfur emissions. The total Arctic sulfate RFari has an interannual variation (relative standard deviation) of 10% among the 5 years. RBU has the largest SO$_2$ emission in 2012, for example, leading to its largest Arctic sulfate RFari contribution in that year. South Asia has its largest contribution to the Arctic sulfate RFari in 2013, rather than 2014 when both the annual and JJA emissions are strongest. These results indicate that for sources within or near the Arctic, emission variability dominates the interannual variations of source contributions to the Arctic sulfate RFari, while interannual variations of remote source contributions are strongly influenced by changes in meteorology.

Future reductions in anthropogenic SO$_2$ emissions for air quality improvement can influence the Arctic climate through changing the sulfate RFari. Figure 11 shows the differences in source contributions to TOA sulfate RFari between the base simulation and a sensitivity simulation with a 20% reduction in anthropogenic SO$_2$ emissions globally. The 20% reduction leads to a net $+0.019$ W m^{-2} increase of TOA radiative flux. All the anthropogenic source regions contribute a positive RFari (i.e., a reduced cooling forcing as compared to the base case) due to the emission reduction, in proportion to their contributions to the total Arctic anthropogenic sulfate RFari (Figure 9). East Asia, especially China, is expected to largely decrease its SO$_2$ emissions in the near future to mitigate air pollution. The 20% emission reduction can lead to a larger warming effect contributed by East Asia than other source regions. Considering that the underestimation of China sulfate concentration by a factor of 2 in CAM5 (Yang, Wang, Smith, Easter, et al., 2017) may lead to an
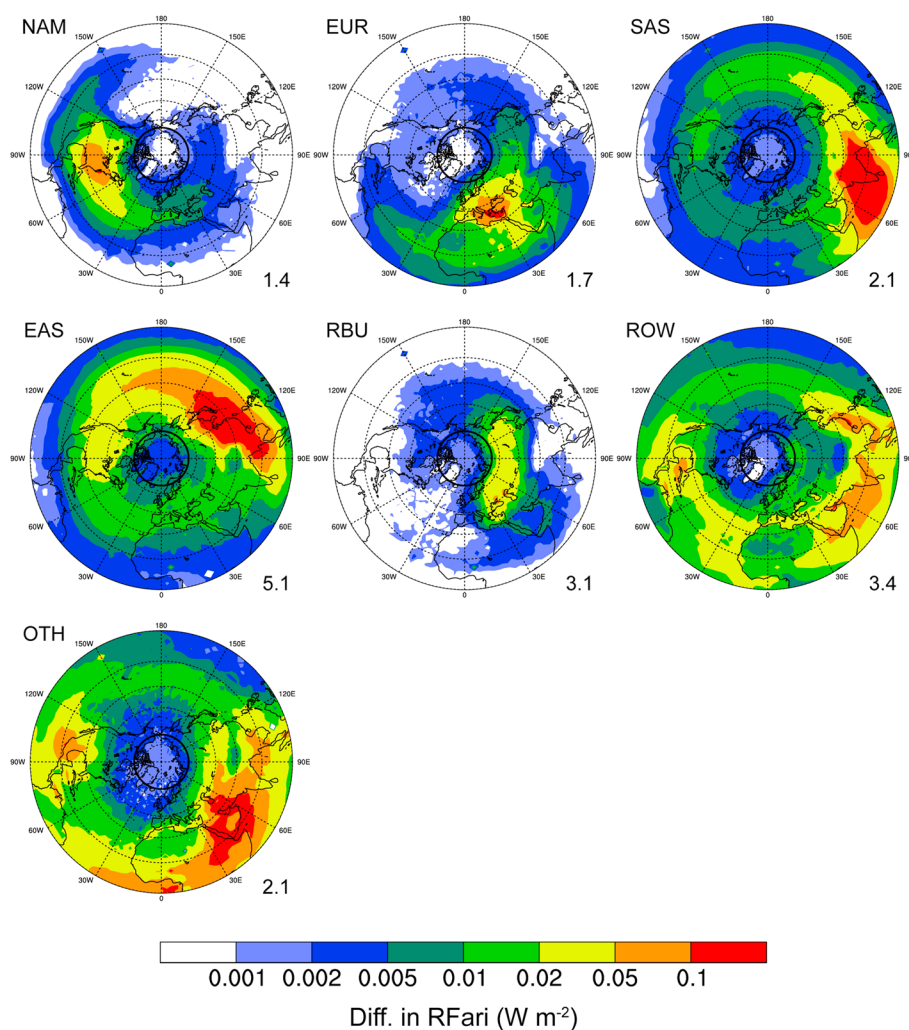
Figure 11. Differences in contributions to annual mean Arctic sulfate RFari (W m^{-2}) from individual anthropogenic source regions at the TOA due to a 20% reduction of anthropogenic SO$_2$ emissions. Arctic mean values (mW m^{-2}) are shown at the bottom right of each panel. Sources with differences less than 1.0 mW m^{-2} are combined and shown as OTH.

underestimation of sulfate transported from China to the Arctic, the warming effect from China emission reductions could be even stronger than our current estimates. A joint reduction in BC emissions could reduce the possible inadvertent Arctic warming from future SO$_2$ emission reductions.

An Arctic forcing efficiency metric, defined as the annual mean TOA RFari contribution divided by the corresponding regional emission, can be used to quantify the sensitivity of Arctic sulfate RFari to specific emission source regions. Figure 12 shows that RBU sources have the largest Arctic RFari efficiency because of their neighboring location. The relatively short transport pathways for emissions from North America and Europe also lead to higher RFari efficiencies for these two source regions. Dry conditions in Central Asia result in a long sulfate lifetime and thus a high Arctic RFari efficiency. The RFari efficiencies calculated from the sensitivity simulation with 80% of the original anthropogenic SO$_2$ emissions are similar to efficiencies calculated from the base simulation, suggesting that the efficiencies do not change much with a relatively small emission perturbation.

To put these results into context, we present an illustrative calculation of the impact of sulfate and BC on equilibrium Arctic surface temperatures. The Arctic equilibrium temperature response to RFari in different source regions is estimated using Arctic climate sensitivity factors for different latitudinal bands from Sand et al. (2016). Note that the Arctic region is defined as 60°N–90°N for this calculation, corresponding to the definition of the Arctic climate sensitivity factors. This method has been used in many previous studies
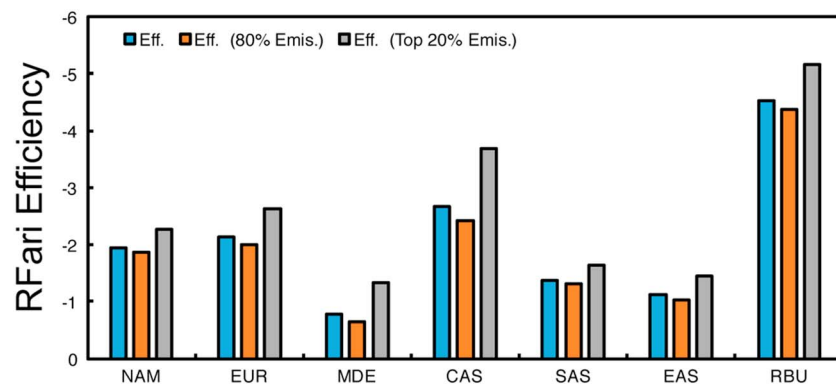
Figure 12. Annual mean Arctic sulfate RFari efficiency (mW m^{-2} (Tg S yr^{-1})$^{-1}$) of the tagged source regions/sectors calculated for the base simulation (blue bars), the sensitivity simulation with a 20% reduction in anthropogenic SO$_2$ emissions (orange bars), and the difference in RFari between the two simulations divided by the corresponding 20% emissions (gray bars). The sulfate RFari efficiency is defined as the annual mean contribution to Arctic sulfate RFari at the TOA divided by the corresponding SO$_2$ emissions. Only the top seven RFari efficiencies in the Northern Hemisphere are shown here.

(Breider et al., 2017; Collins et al., 2013; Flanner, 2013; Sand et al., 2016; Shindell & Faluvegi, 2009). We estimate the temperature impact of Arctic local BC RFari using a different method. While the impact of BC on Arctic surface temperature depends on altitude (Flanner, 2013), vertically resolved forcing was not calculated in our simulations. Thus, a vertically integrated temperature-forcing relationship from Shindell and Faluvegi (2009) is used to estimate temperature impact of Arctic BC forcing. Table S5 shows these factors for BC and sulfate RFari at different latitudinal bands. The estimated equilibrium Arctic surface temperature response to global anthropogenic sulfate (Table 2) RFari is −0.19 K. Emissions in East Asia contribute −0.05 K to the Arctic surface temperature response, mainly due to its sulfate RFari over 28°N–60°N, followed by −0.01 to −0.03 K due to sources from ROW (including the Arctic), South Asia, the Middle East, Europe, and North America. In comparison, BC RFari leads to a +0.33 K Arctic surface temperature response, which is partly offset by sulfate RFari. BC albedo feedback on snow and ice is not included in this estimate and would add additional warming.

6. Conclusion and Discussion

Source attributions of Arctic sulfate and RFari for 2010–2014 are quantified using the CESM with a sulfur source-tagging technique. Following a previous study (Yang, Wang, Smith, Easter, et al., 2017) that examined the global source-receptor relationship of sulfate, 14 source regions and two natural sectors are tagged. The

Table 2
Arctic Surface Temperature Response (K) to Sulfate and Black Carbon Radiative Forcing Due to Aerosol-Radiation Interactions

Forcing location	NAM	CAM	SAM	EUR	NAF	SAF	MDE	SEA
60°N–90°N	−2.8E−03	−9.1E−05	1.1E−04	−3.6E−03	−4.5E−05	6.7E−05	−1.2E−03	−1.0E−04
28°N–60°N	−9.4E−03	−1.4E−03	1.3E−04	−9.7E−03	−1.2E−03	3.8E−05	−7.1E−03	−2.7E−04
28°S–28°N	−1.4E−03	−2.9E−03	−3.3E−03	−2.1E−03	−1.4E−03	−6.4E−03	−7.5E−03	−2.5E−03
90°S–28°S	3.3E−05	7.3E−06	−4.8E−04	3.3E−05	3.7E−05	−9.5E−04	2.9E−06	−7.6E−05
Total	−1.4E−02	−4.5E−03	−3.5E−03	−1.5E−02	−2.5E−03	−7.3E−03	−1.6E−02	−3.0E−03

Forcing location	CAS	SAS	EAS	RBU	PAN	ROW	Sulfate	BC
60°N–90°N	−1.3E−03	−3.4E−03	−8.3E−03	−7.0E−03	1.7E−04	−6.3E−03	−3.4E−02	−2.4E−02
28°N–60°N	−3.1E−03	−7.9E−03	−2.9E−02	−7.4E−03	2.0E−04	−1.0E−02	−8.6E−02	1.1E−01
28°S–28°N	−7.6E−04	−1.2E−02	−1.1E−02	−6.4E−04	−8.9E−04	−1.3E−02	−6.5E−02	2.4E−01
90°S–28°S	3.6E−05	−1.8E−04	−3.3E−04	3.8E−05	−2.6E−04	−5.6E−04	−2.7E−03	6.3E−03
Total	−5.1E−03	−2.4E−02	−4.8E−02	−1.5E−02	−7.8E−04	−3.0E−02	−1.9E−01	3.3E−01

Note. The Arctic region is defined as 60°N–90°N here. BC = black carbon; CAM = Central America; CAS = Central Asia; EAS = East Asia; EUR = Europe; MDE = the Middle East; NAF = North Africa; NAM = North America; PAN = Pacific/Australia/New Zealand; RBU = Russia/Belarus/Ukraine; SAF = Southern Africa; SAM = South America; SAS = South Asia; SEA = Southeast Asia; ROW = rest of the world.

Arctic was generally defined as 66.5°N–90°N in this work. Results show that regions with high emissions and/or near/within the Arctic have large contributions to the Arctic sulfate burden. Sources from East Asia have the largest contribution to the Arctic sulfate column burden, with an annual mean contribution of 27%, followed by 11–13% each from South Asia, ROW (including the Arctic), and RBU sources. Natural sources contribute 13% of the Arctic sulfate burden. Unlike the column burden, 50% of the near-surface concentrations are from Arctic local emissions (part of the ROW region), followed by RBU and DMS sources.

Different source regions contribute distinct vertical distributions. Distant source regions have larger Arctic sulfate contributions at higher altitudes. East Asia and South Asia have their maximum of contributions at 9–12 km, whereas sources from ROW (dominated by Arctic sources) and RBU account largely for the Arctic sulfate below 2 km.

Meteorology has a strong impact on the seasonality of contributions from emission sources outside the Arctic, with meteorological effects largely determining the seasonal contribution pattern from remote regions. The location of the Arctic front has a large influence on nearby emissions, for example, the RBU region, as also found for BC by Stohl et al. (2013).

Anthropogenic sulfate gives a negative RFari of -0.07 W m^{-2} at the Arctic surface, largely offsetting the positive forcing from BC-in-snow heating. Sulfate RFari is -0.08 W m^{-2} at the TOA, offsetting one third of the positive TOA RFari from atmospheric BC, indicating that sulfate aerosol is an important direct influence on Arctic climate. We find that the absolute magnitude of sulfate forcing increases relative to that of BC when a larger Arctic region is considered (60°N–90°N). This means that a larger portion of BC positive forcing is being offset by sulfate cooling at lower Arctic latitudes.

Sources from East Asia, ROW (dominated by local Arctic sources), and RBU contribute -0.020, -0.016, and -0.014 W m^{-2}, respectively, to the total Arctic sulfate RFari at the TOA, followed by between -0.006 and -0.009 W m^{-2} from North America, Europe, and South Asia. Natural sources including oceanic DMS emissions and volcanic emissions account for -0.010 W m^{-2}.

Almost all source regions/sectors show a seasonal sulfate TOA RFari contribution peaks in JJA when insolation is the strongest. In JJA, emissions from distant East Asia, neighboring sources in RBU, and local Arctic sources (in ROW) have similar contributions of -0.035 to -0.045 W m^{-2} to the Arctic sulfate RFari, indicating that both location and emission strength of source regions are important to the Arctic sulfate RFari. In the 5 years (2010–2014) simulated in this study, total Arctic sulfate RFari has an interannual variation of 10%. For sources within or near the Arctic, emission variability dominates the interannual variations in source contributions to the Arctic sulfate RFari, while interannual variations of remote source contributions are more influenced by meteorological changes.

A 20% reduction in anthropogenic SO$_2$ emissions leads to a net $+0.019$ W m^{-2} increase of radiative flux at the Arctic TOA, with the largest contribution from East Asia source, which is expected to largely decrease in near future to mitigate aerosol pollution problems. Overall, reductions in BC emissions might be able to prevent inadvertent Arctic warming from future reductions in SO$_2$ emissions.

Results suggest that source emissions near the Arctic together with meteorology favoring a longer lifetime is more efficient in influencing Arctic sulfate RFari. Arctic sulfate RFari efficiency, defined as the Arctic TOA RFari induced per unit source emission, is largest for RBU sources because of their neighboring location. Shorter transport pathways and/or less efficient wet removal also lead to relatively high RFari efficiencies for North America, Europe, and Central Asia.

Using equilibrium Arctic climate sensitivity factors from previous studies, anthropogenic sulfate results in 0.19 K of Arctic (here 60°N–90°N) cooling, with the largest response from sulfate RFari over midlatitudes of the Northern Hemisphere (e.g., East Asia). Arctic local forcing from atmospheric BC produces a cooling; however, warming from remote BC results in a net positive $+0.33$ K Arctic surface temperature response (not including snow/ice feedbacks), which is partly offset by sulfate cooling.

It is challenging for global models to accurately capture both the seasonality and magnitude of Arctic sulfate concentrations (Shindell et al., 2008). Compared to surface sulfate observations in the Arctic, our CAM5 simulation roughly reproduces the seasonal pattern. The simulation overestimates concentrations at two of four sites (Zeppelin and Trapper Creek) in late spring and early summer. In JJA, DMS contributes more than 50% to

surface sulfate at the Zeppelin site, pointing to a potential overestimation of the exogenous DMS emission fields used in our simulations. In line with the results from Breider et al. (2017), we conclude that accurate DMS emissions are important in simulating sulfate concentrations at this site.

At the Trapper Creek site in Alaska, sulfate concentrations are overestimated by the model, as also found by Breider et al. (2014). At the Alert site, our model catches the minimum in JJA but strongly underestimates the concentrations in other seasons, which has also been reported by many other modeling studies (Breider et al., 2014, 2017; Eckhardt et al., 2015; Fisher et al., 2011). However, it is challenging to pinpoint the source of this difference because no source region shows a dominant contribution at this site.

Overall, the results of these comparisons are mixed, with both overestimates and underestimates. Over summer, which dominates sulfate forcing over the Arctic, the model seems to do well for the anthropogenic component of emissions except for the Trapper Creek site, where the global model likely cannot capture the influence of the complex topography there. Spatial downscaling of the model results would be useful to improve model/site-data comparisons.

Note that differences in emission data sets, SO_2 injection height, model physics, and meteorology can all cause a disagreement in the source attribution of sulfate between models. In areas with complex topography or large gradients in emissions, comparing point measurements can also be problematic. Eckhardt et al. (2015) evaluated the aerosol simulation in the Arctic by multiple models and concluded that no class of models performed substantially better than the others, and differences in model performance were largely attributed to the treatment of aerosol removal in the models. Table S6 compares the column burden and deposition of sulfate over the whole globe and the Arctic in this study with those from Breider et al. (2017). The annual sulfate deposition shows large differences between the two studies, due to differences in emissions, model physics, and the Arctic latitude range. The difference in wet deposition leads to different burdens.

Forcing due to aerosol-cloud interactions may also influence the Arctic, but it is not specifically analyzed in this study due to large uncertainties in the treatment of Arctic clouds and cloud-aerosol interactions in climate models (McFarquhar et al., 2011). Aerosols can also influence poleward heat transport, which may also have a substantial influence on the Arctic energy balance (Sand et al., 2013) but is not considered in this source attribution study.

References

Acosta Navarro, J. C., Varma, V., Riipinen, I., Seland, Ø., Kirkevåg, A., Struthers, H., … Ekman, A. M. L. (2016). Amplification of Arctic warming by past air pollution reductions in Europe. *Nature Geoscience*, *9*(4), 277–281. https://doi.org/10.1038/ngeo2673

AMAP (2015). AMAP assessment 2015: Black carbon and ozone as Arctic climate forcers. Arctic Monitoring and Assessment Programme (AMAP) (pp. Vii + 116) Oslo, Norway.

Breider, T. J., Mickley, L. J., Jacob, D. J., Ge, C., Wang, J., Payer Sulprizio, M., … Hopke, P. K. (2017). Multidecadal trends in aerosol radiative forcing over the Arctic: Contribution of changes in anthropogenic aerosol to Arctic warming since 1980. *Journal of Geophysical Research: Atmospheres*, *122*, 3573–3594. https://doi.org/10.1002/2016JD025321

Breider, T. J., Mickley, L. J., Jacob, D. J., Wang, Q., Fisher, J. A., Chang, R. Y.-W., & Alexander, B. (2014). Annual distributions and sources of Arctic aerosol components, aerosol optical depth, and aerosol absorption. *Journal of Geophysical Research: Atmospheres*, *119*, 4107–4124. https://doi.org/10.1002/2013JD020996

Collins, W. J., Fry, M. M., Yu, H., Fuglestvedt, J. S., Shindell, D. T., & West, J. J. (2013). Global and regional temperature-change potentials for near-term climate forcers. *Atmospheric Chemistry and Physics*, *13*(5), 2471–2485. https://doi.org/10.5194/acp-13-2471-2013

Dawson, J. P., Adams, P. J., & Pandis, S. N. (2007). Sensitivity of PM2.5 to climate in the eastern US: A modeling case study. *Atmospheric Chemistry and Physics*, *7*, 4295–4309. https://doi.org/10.1059/acp-7-4295-2007

Diehl, T. (2009). A global inventory of volcanic SO2 emissions for hindcast scenarios. Retrieved from http://aerocom.met.no/download/emissions/AEROCOM_HC/volc/, last accessed on 05 2017.

Eckhardt, S., Quennehen, B., Olivié, D. J. L., Berntsen, T. K., Cherian, R., Christensen, J. H., … Stohl, A. (2015). Current model capabilities for simulating black carbon and sulfate concentrations in the Arctic atmosphere: A multi-model evaluation using a comprehensive measurement data set. *Atmospheric Chemistry and Physics*, *15*(16), 9413–9433. https://doi.org/10.5194/acp-15-9413-2015

Fisher, J. A., Jacob, D. J., Wang, Q., Bahreini, R., Carouge, C. C., Cubison, M. J., … Yantosca, R. M. (2011). Sources, distribution, and acidity of sulfate–ammonium aerosol in the Arctic in winter–spring. *Atmospheric Environment*, *45*, 7301–7318. https://doi.org/10.1016/j.atmosenv.2011.08.030

Flanner, M. G. (2013). Arctic climate sensitivity to local black carbon. *Journal of Geophysical Research: Atmospheres*, *118*, 1840–1851. https://doi.org/10.1002/jgrd.50176

Flanner, M. G., Zender, C. S., Randerson, J. T., & Rasch, P. J. (2007). Present day climate forcing and response from black carbon in snow. *Journal of Geophysical Research*, *112*, D11202. https://doi.org/10.1029/2006JD008003

Fyfe, J. C., von Salzen, K., Gillett, N. P., Arora, V. K., Flato, G. M., & McConnell, J. R. (2013). One hundred years of Arctic surface temperature variation due to anthropogenic influence. *Scientific Reports*, *3*(1), 2645. https://doi.org/10.1038/srep02645

Gagné, M.-È., Gillett, N. P., & Fyfe, J. C. (2015). Impact of aerosol emission controls on future Arctic sea ice cover. *Geophysical Research Letters*, *42*, 8481–8488. https://doi.org/10.1002/2015GL065504

Garrett, T. J., Brattström, S., Sharma, S., Worthy, D. E. J., & Novelli, P. (2011). The role of scavenging in the seasonal transport of black carbon and sulfate to the Arctic. *Geophysical Research Letters*, *38*, L16805. https://doi.org/10.1029/2011GL048221

Ghan, S. J. (2013). Technical note: Estimating aerosol effects on cloud radiative forcing. *Atmospheric Chemistry and Physics*, *13*(19), 9971–9974. https://doi.org/10.5194/acp-13-9971-2013

Ghan, S. J., & Zaveri, R. A. (2007). Parameterization of optical properties for hydrated internally mixed aerosol. *Journal of Geophysical Research*, *112*, D10201. https://doi.org/10.1029/2006JD007927

Gong, S. L., Zhao, T. L., Sharma, S., Toom-Sauntry, D., Lavoué, D., Zhang, X. B., … Barrie, L. A. (2010). Identification of trends and interannual variability of sulfate and black carbon in the Canadian High Arctic: 1981–2007. *Journal of Geophysical Research*, *115*, D07305. https://doi.org/10.1029/2009JD012943

Hegg, D. A., Warren, S. G., Grenfell, T. C., Doherty, S. J., & Clarke, A. D. (2010). Sources of light-absorbing aerosol in arctic snow and their seasonal variation. *Atmospheric Chemistry and Physics*, *10*, 10,923–10,938. https://doi.org/10.5194/acp-10-10923-2010

Hoesly, R. M., Smith, S. J., Feng, L., Klimont, Z., Janssens-Maenhout, G., Pitkanen, T., … Zhang, Q. (2018). Historical (1750–2014) anthropogenic emissions of reactive gases and aerosols from the Community Emission Data System (CEDS). *Geoscientific Model Development*, *11*, 369–408. https://doi.org/10.5194/gmd-11-369-2018

Intergovernmental Panel on Climate Change (IPCC) (2013). *Climate Change 2013: The Physical Science Basis. Contribution of Working Group I to the Fifth Assessment Report of the Intergovernmental Panel on Climate Change* (p. 1535). Cambridge, UK: Cambridge University Press.

Jacob, D. J., Crawford, J. H., Maring, H., Clarke, A. D., Dibb, J. E., Emmons, L. K., … Singh, H. B. (2010). The arctic research of the composition of the troposphere from aircraft and satellites (ARCTAS) mission: Design, execution, and first results. *Atmospheric Chemistry and Physics*, *10*(11), 5191–5212. https://doi.org/10.5194/acp-10-5191-2010

Jacobson, M. Z. (2010). Short-term effects of controlling fossil-fuel soot, biofuel soot and gases, and methane on climate, arctic ice, and air pollution health. *Journal of Geophysical Research*, *115*, D14209. https://doi.org/10.1029/2009JD013795

Koch, D., Schulz, M., Kinne, S., McNaughton, C., Spackman, J. R., Balkanski, Y., … Zhao, Y. (2009). Evaluation of black carbon estimations in global aerosol models. *Atmospheric Chemistry and Physics*, *9*, 9001–9026. https://doi.org/10.5194/acp-9-9001-2009

Law, K. S., & Stohl, A. (2007). Arctic air pollution: Origins and impacts. *Science*, *315*, 1537–1540. https://doi.org/10.1126/science.1137695

Li, C., Joiner, J., Krotkov, N. A., & Bhartia, P. K. (2013). A fast and sensitive new satellite SO_2 retrieval algorithm based on principal component analysis: Application to the ozone monitoring instrument. *Geophysical Research Letters*, *40*, 6314–6318. https://doi.org/10.1002/2013GL058134

Liu, X., Easter, R. C., Ghan, S. J., Zaveri, R., Rasch, P., Shi, X., … Mitchell, D. (2012). Toward a minimal representation of aerosols in climate models: Description and evaluation in the Community Atmosphere Model CAM5. *Geoscientific Model Development*, *5*, 709–739. https://doi.org/10.5194/gmd-5-709-2012

Ma, P.-L., Rasch, P. J., Wang, H., Zhang, K., Easter, R. C., Tilmes, S., … Lamarque, J.-F. (2013). The role of circulation features on black carbon transport into the Arctic in the Community Atmosphere Model version 5 (CAM5). *Journal of Geophysical Research: Atmospheres*, *118*, 4657–4669. https://doi.org/10.1002/jgrd.50411

Mahmood, R., von Salzen, K., Flanner, M., Sand, M., Langner, J., Wang, H., & Huang, L. (2016). Seasonality of global and Arctic black carbon processes in the Arctic Monitoring and Assessment Programme models. *Journal of Geophysical Research: Atmospheres*, *121*, 7100–7116. https://doi.org/10.1002/2016JD024849

McFarquhar, G. M., Ghan, S., Verlinde, J., Korolev, A., Strapp, J. W., Schmid, B., … Glen, A. (2011). Indirect and Semi-Direct Aerosol Campaign (ISDAC): The impact of Arctic aerosols on clouds. *Bulletin of the American Meteorological Society*, *92*, 183–201. https://doi.org/10.1175/2010BAMS2935.1

Myhre, G., Samset, B. H., Schulz, M., Balkanski, Y., Bauer, S., Berntsen, T. K., … Zhou, C. (2013). Radiative forcing of the direct aerosol effect from AeroCom phase II simulations. *Atmospheric Chemistry and Physics*, *13*(4), 1853–1877. https://doi.org/10.5194/acp-13-1853-2013

Neale, R. B., Chen, C. C., Gettelman, A., Lauritzen, P. H., Park, S., Williamson, D. L., … Taylor, M. A. (2012). Description of the NCAR Community Atmosphere Model (CAM 5.0) (NCAR Tech. Note NCAR/TN-485CSTR pp. 289). Boulder, CO: National Center for Atmospheric Research.

Qian, Y., Yasunari, T. J., Doherty, S. J., Flanner, M. G., Lau, W. K. M., Ming, J., … Zhang, R. (2015). Light-absorbing particles in snow and ice: Measurement and modeling of climatic and hydrological impact. *Advances in Atmospheric Sciences*, *32*(1), 64–91. https://doi.org/10.1007/s00376-014-0010-0

Quinn, P. K., Bates, T. S., Baum, E., Doubleday, N., Fiore, A. M., Flanner, M., … Warren, S. G. (2008). Short-lived pollutants in the Arctic: Their climate impact and possible mitigation strategies. *Atmospheric Chemistry and Physics*, *8*, 1723–1735. https://doi.org/10.5194/acp-8-1723-2008

Quinn, P. K., Shaw, G., Andrews, E., Dutton, E. G., Ruoho-Airola, T., & Gong, S. L. (2007). Arctic haze: Current trends and knowledge gaps. *Tellus B*, *59*, 115–129. https://doi.org/10.1111/j.1600-0889.2006.00238.x

Rao, S., Klimont, Z., Smith, S. J., van Dingenen, R., Dentener, F., Bouwman, L., … Tavoni, M. (2017). Future air pollution in the shared socio-economic pathways. *Global Environmental Change*, *42*, 346–358. https://doi.org/10.1016/j.gloenvcha.2016.05.012

Rienecker, M. M., Suarez, M. J., Gelaro, R., Todling, R., Bacmeister, J., Liu, E., … Woollen, J. (2011). MERRA: NASA's modern-era retrospective analysis for research and applications. *Journal of Climate*, *24*, 3624–3648. https://doi.org/10.1175/JCLI-D-11-00015.1

Sand, M., Berntsen, T. K., Kay, J. E., Lamarque, J. F., Seland, Ø., & Kirkevåg, A. (2013). The Arctic response to remote and local forcing of black carbon. *Atmospheric Chemistry and Physics*, *13*(1), 211–224. https://doi.org/10.5194/acp-13-211-2013

Sand, M., Berntsen, T. K., von Salzen, K., Flanner, M. G., Langner, J., & Victor, D. G. (2016). Response of arctic temperature to changes in emissions of short-lived climate forcers. *Nature Climate Change*, *6*(3), 286–289. https://doi.org/10.1038/nclimate2880

Sharma, S., Andrews, E., Barrie, L. A., Ogren, J. A., & Lavoué, D. (2006). Variations and sources of the equivalent black carbon in the high Arctic revealed by long-term observations at Alert and Barrow: 1989–2003. *Journal of Geophysical Research*, *111*, D14208. https://doi.org/10.1029/2005JD006581

Shaw, G. E. (1995). The Arctic haze phenomenon. *Bulletin of the American Meteorological Society*, *76*(12), 2403–2413. https://doi.org/10.1175/1520-0477(1995)076%3C2403:TAHP%3E2.0.CO;2

Shindell, D., & Faluvegi, G. (2009). Climate response to regional radiative forcing during the twentieth century. *Nature Geoscience*, *2*, 294–300. https://doi.org/10.1038/ngeo473

Shindell, D. T., Chin, M., Dentener, F., Doherty, R. M., Faluvegi, G., Fiore, A. M., … Zuber, A. (2008). A multi-model assessment of pollution transport to the Arctic. *Atmospheric Chemistry and Physics*, *8*, 5353–5372. https://doi.org/10.5194/acp-8-5353-2008

Smith, S. J., van Aardenne, J., Klimont, Z., Andres, R. J., Volke, A., & Delgado Arias, S. (2011). Anthropogenic sulfur dioxide emissions: 1850–2005. *Atmospheric Chemistry and Physics*, *11*, 1101–1116. https://doi.org/10.5194/acp-11-1101-2011

Stjern, C. W., Samset, B. H., Myhre, G., Bian, H., Chin, M., Davila, Y., … Tilmes, S. (2016). Global and regional radiative forcing from 20% reductions in BC, OC and SO_4 – An HTAP2 multi-model study. *Atmospheric Chemistry and Physics*, *16*(21), 13,579–13,599. https://doi.org/10.5194/acp-16-13579-2016

Stohl, A. (2006). Characteristics of atmospheric transport into the Arctic troposphere. *Journal of Geophysical Research*, *111*, D11306. https://doi.org/10.1029/2005JD006888

Stohl, A., Klimont, Z., Eckhardt, S., Kupiainen, K., Shevchenko, V. P., Kopeikin, V. M., & Novigatsky, A. N. (2013). Black carbon in the Arctic: The underestimated role of gas flaring and residential combustion emissions. *Atmospheric Chemistry and Physics*, *13*(17), 8833–8855. https://doi.org/10.5194/acp-13-8833-2013

US Environmental Protection Agency (2010). *Our Nation's Air – Status and Trends Through 2008*. Washington, DC: American Geophysical Union.

van der A, R. J., Mijling, B., Ding, J., Koukouli, M. E., Liu, F., Li, Q., … Theys, N. (2017). Cleaning up the air: Effectiveness of air quality policy for SO_2 and NO_x emissions in China. *Atmospheric Chemistry and Physics*, *17*(3), 1775–1789. https://doi.org/10.5194/acp-17-1775-2017

van Marle, M. J. E., Kloster, S., Magi, B. I., Marlon, J. R., Daniau, A. L., Field, R. D., … van der Werf, G. R. (2017). Historic global biomass burning emissions for CMIP6 (BB4CMIP) based on merging satellite observations with proxies and fire models (1750–2015). *Geoscientific Model Development*, *10*(9), 3329–3357. https://doi.org/10.5194/gmd-10-3329-2017

Vestreng, V., Myhre, G., Fagerli, H., Reis, S., & Tarrasón, L. (2007). Twenty-five years of continuous sulphur dioxide emission reduction in Europe. *Atmospheric Chemistry and Physics*, *7*, 3663–3681. https://doi.org/10.5194/acp-7-3663-2007

Wang, H., Easter, R. C., Rasch, P. J., Wang, M., Liu, X., Ghan, S. J., … Vinoj, V. (2013). Sensitivity of remote aerosol distributions to representation of cloud–aerosol interactions in a global climate model. *Geoscientific Model Development*, *6*(3), 765–782. https://doi.org/10.5194/gmd-6-765-2013

Wang, H., Rasch, P. J., Easter, R. C., Singh, B., Zhang, R., Ma, P.-L., … Beagley, N. (2014). Using an explicit emission tagging method in global modeling of source-receptor relationships for black carbon in the Arctic: Variations, sources, and transport pathways. *Journal of Geophysical Research: Atmospheres*, *119*, 12,888–12,909. https://doi.org/10.1002/2014JD022297

Wobus, C., Flanner, M., Sarofim, M. C., Moura, M. C. P., & Smith, S. J. (2016). Future Arctic temperature change resulting from a range of aerosol emissions scenarios. *Earth's Future*, *4*(6), 270–281. https://doi.org/10.1002/2016EF000361

Yang, Q., Bitz, C. M., & Doherty, S. J. (2014). Offsetting effects of aerosols on Arctic and global climate in the late 20th century. *Atmospheric Chemistry and Physics*, *14*(8), 3969–3975. https://doi.org/10.5194/acp-14-3969-2014

Yang, Y., Wang, H., Smith, S. J., Easter, R., Ma, P.-L., Qian, Y., … Rasch, P. J. (2017). Global source attribution of sulfate concentration, direct and indirect radiative forcing. *Atmospheric Chemistry and Physics*, *17*(14), 8903–8922. https://doi.org/10.5194/acp-17-8903-2017

Yang, Y., Wang, H., Smith, S. J., Ma, P.-L., & Rasch, P. J. (2017). Source attribution of black carbon and its direct radiative forcing in China. *Atmospheric Chemistry and Physics*, *17*(6), 4319–4336. https://doi.org/10.5194/acp-17-4319-2017

Zhang, K., Wan, H., Liu, X., Ghan, S. J., Kooperman, G. J., Ma, P.-L., … Lohmann, U. (2014). Technical note: On the use of nudging for aerosol–climate model intercomparison studies. *Atmospheric Chemistry and Physics*, *14*(16), 8631–8645. https://doi.org/10.5194/acp-14-8631-2014